Automated Pneumatic Shuttle for Magnetic Field Cycling and Parahydrogen Hyperpolarized Multidimensional NMR

Patrick TomHona,*, Evan Akeroyda, Sören Lehmkuhla, Eduard Y. Chekmenev, c,d and Thomas Theisa,b*

- ^a Department of Chemistry, North Carolina State University, Raleigh, NC 27606, United States
- ^b Joint Department of Biomedical Engineering, University of North Carolina, Chapel Hill, NC, and North Carolina State University, Raleigh, NC 27606, United States
- ^c Department of Chemistry, Integrative Biosciences (Ibio), Wayne State University, Karmanos Cancer Institute (KCI), Detroit, MI 48202, United States
- ^d Russian Academy of Sciences, Leninskiy Prospekt 14, 119991 Moscow, Russia

We present a simple-to-implement pneumatic sample shuttle for automation of magnetic field cycling and multidimensional NMR. The shuttle system is robust allowing automation of hyperpolarized and non-hyperpolarized measurements, including variable field lifetime measurements, SABRE polarization optimization, and SABRE multidimensional experiments. Relaxation-protected singlet states are evaluated by variable-field T_1 and T_2 measurements. Automated shuttling facilitates characterization of hyperpolarization dynamics, field dependence and polarization buildup rates. Furthermore, reproducible hyperpolarization levels at every shuttling event enables automated 2D hyperpolarized NMR, including the first inverse 15 N/ 1 H HSQC. We uncover binding mechanisms of the catalytic species through cross peaks that are not accessible in standard one-dimensional hyperpolarized experiments. The simple design of the shuttling setup interfaced with standard TTL signals allows easy adaptation to any standard NMR magnet.

1. Introduction

Nuclear magnetic resonance (NMR) is an invaluable tool to provide a wealth of chemical, structural, and spatial information. Traditional NMR is limited by low thermal spin polarization, reducing sensitivity and requiring large superconducting magnets for NMR spectroscopy and imaging. Hyperpolarization methods overcome the traditional sensitivity limitations of NMR, perturbing nuclear spin populations from their thermal equilibrium [1–4]. Signal amplification by reversible exchange (SABRE) is a parahydrogen-based [5] method that uses an organometallic catalyst to transfer spin order from p-H $_2$ to target substrates [6,7]. However, with most existing approaches, hyperpolarization is a transient feature precluding averaging and multi-scan experiments, such as multidimensional NMR. Here, we present an approach for robust static magnetic field cycling of thermally polarized and SABRE-rehyperpolarized samples, enabling reliable averaging of hyperpolarized experiments as well as hyperpolarized multidimensional NMR spectroscopy. The described apparatus was employed to measure proton singlet state lifetimes of common drugs, evaluate hyperpolarization dynamics, and conduct multidimensional NMR, including inverse 15 N/ 1 H HSQC and 1 H COSY, to reveal new SABRE binding mechanisms.

SABRE is a simple, cost-effective hyperpolarization method that can achieve polarization levels >30% in ideal cases using a simple experimental design [8–11]. However, under standard bubbling setups polarization levels between 1% and 10% are typical. Investigation of both the spin physics and chemistry of this phenomenon has yielded a rich field accessing hyperpolarization of a wide variety of substrate molecules [6,8,12–16]. Polarization transfer from parahydrogen (p-H $_2$) to target substrates in a SABRE complex is optimized at a level anti-crossing (LAC) in the strong coupling regime [17–20]. Polarization can flow freely through the J-coupling network of the catalyst, generating spin mixing between the p-H $_2$ singlet and unpolarized substrate. SABRE hyperpolarization relies on a continuous refreshment of p-H $_2$ in solution, therefore polarization can be continuously generated in the same sample [21–29]. Therefore, the SABRE process requires consideration of not only the quantum mechanics and chemistry, but also of the engineering to continuously refresh p-H $_2$ in solution while field cycling the sample [30].

In the development of SABRE spin physics, various methods have been employed to introduce p- H_2 in solution while field cycling the sample to access high polarization levels. On the one hand, in so-called shake and drop experiments, the NMR tube is first pressurized with p- H_2 and then shaken in either a fringe magnetic field [6,31] or magnet array [32]. While shake and drop experiments introduce large quantities of fresh p- H_2 to the polarization transfer catalyst at once, reproducibility is limited due to sample manipulation. On the other hand, bubble and transfer experiments

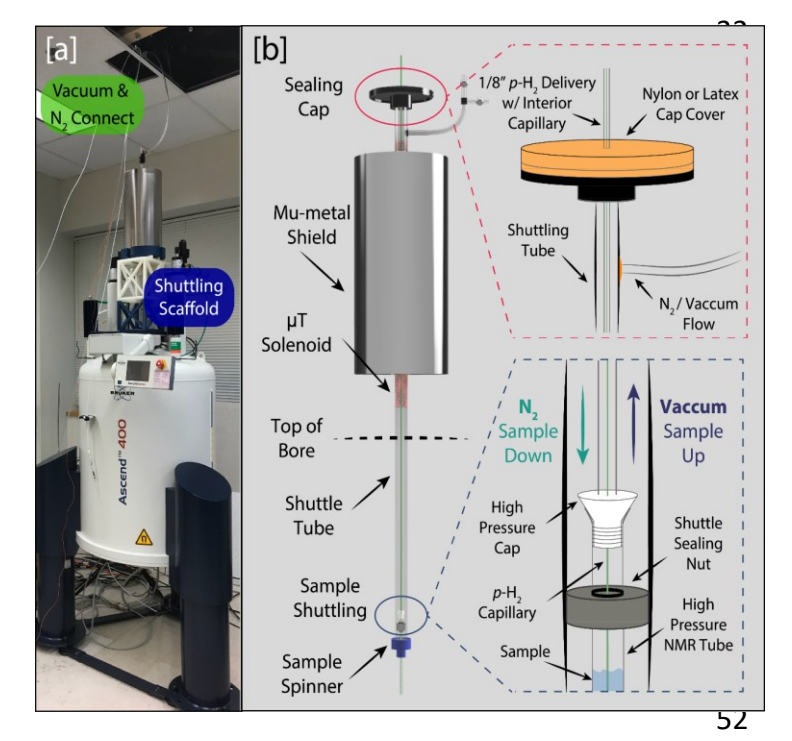


Fig. 1 Pneumatic shuttling system for robust automated SABRE experiments. (a) Bruker Ascend 400 MHz magnet with self-assembled 50% parahydrogen generator and SABRE-SHEATH shuttling setup with mu-metal shield to access microtesla (μ T) regime. (b) 3D CAD rendering of the shuttling setup. Diagram is to scale with exception of the length shuttling tube. See supporting information for 16.5 mT/A field control unit, as well as exact dimensions of all parts.

[32] are more reproducible but typically give slightly lower polarization. Still, both methods require manual sample transfer to the detection field. Automation is highly desirable to improve reproducibility especially in case of long experimental times.

Continuous flow SABRE [29,33-36] and mechanical field-cycling schemes [17] offer significantly higher reproducibility and throughput. However, continuous flow systems may be limited by line broadening and susceptibility artifacts, while mechanical cycling schemes may be limited by cost and technical complexity [37]. Although ultra-low-field in situ detection of SABRE has been demonstrated, this approach lacks chemical information due to vanishing chemical shift dispersion in ultra-low magnetic fields, e.g. 6 mT [38]. Other approaches to multidimensional PHIP and SABRE experiments have focused on ultrafast methods [39,40] or utilizing flow probes [41]. Also, mechanical, stepper-motor based systems have shown robust, fast field-cycling over a wide field range [42]. Pneumatic field cycling has been implemented for PHIP experiments [43] and zero-field measurements previously [44,45], illustrating fast transfer speeds and ease of implementation. Here we demonstrate a simple-to-implement high-field pneumatic shuttle coupled with SABRE hyperpolarization to for field dependent lifetime (T_1, T_S) measurements as well as robust multidimensional NMR. With these approaches

we gain additional insight into the exchanging catalytic SABRE system by detecting weak binding ligands and elucidating short lived catalytic intermediates.

60

2. Pneumatic Shuttling System Design

We designed a simple pneumatic shuttling setup to address the limitations of manual SABRE hyperpolarization methodologies and provide a robust, high-throughput system that enables multidimensional NMR. While pneumatic systems have previously been developed for DNP [46,47], PHIP [43], and zero-field [44,45], these pneumatic designs have not been implemented with SABRE hyperpolarization at high-field. This automated setup allows for hundreds of SABRE experiments in quick succession and affords control of shuttling speed, p-H $_2$ bubbling rate and bubbling time through samples at adjustable polarization transfer fields, ranging from sub μ T to T strength.

The shuttling is controlled by basic pressure regulation in a confined polycarbonate shuttling tube (5/8" OD, $\frac{1}{2}$ " ID). A membrane vacuum pump (Welch-Ilmvac 2054B-01) provides sufficient vacuum (100 L/min, 8 mbar) to pull the high-pressure sample tube (Wilmad 524-PV-7, rated to 300 psi) up into the desired polarization transfer field. House nitrogen gas pressure is applied to insert the sample tube into the high-field magnet (Bruker 400 MHz with Neo Avance III console) for detection. A Plexiglas nut around the sample tube and a latex covered cap on the shuttle tube create a sealed shuttling atmosphere while allowing for free tube movement, including the 1/8" p-H $_2$ supply/exhaust tube (see below). The house nitrogen line is regulated to pressures of 10 to 15 psi to control the speed of the shuttling. Both the vacuum and nitrogen inputs are buffered through 5-gallon compressed air tanks. Normally-closed valves regulate the application of vacuum or nitrogen pressure. Operating at a nitrogen pressure of 12 psi the sample tube is injected into the magnet in $\sim 0.5 \text{ s}$ and the full applied vacuum shuttles the sample into a desired polarization transfer field in $\sim 1 \text{ s}$ (See Supporting Information S1). An additional settling time of $\sim 1 \text{ s}$ can be used to let the sample and tube stabilize in the probe before detection.

To create a fully automated system, p-H $_2$ bubbling is controlled by a pneumatic valve (Swagelok MS-131-SR) operated by a three-way/two-position air-flow solenoid (Swagelok K-MS-SV-64). All three system solenoids are controlled through inversion of positive TTL outputs from the Bruker Neo Avance III console (See Supporting Information S2). Bubbling is implemented through a tube-in-tube design as follows; p-H $_2$ flows through an interior capillary tubing and then bubbles are regulated through back pressure in the exterior 1/8" PTFE tubing up to 300 psi. In this paper, we use 50% p-H $_2$ produced with an inexpensive, easily established design flowing H $_2$ over iron oxide at 77 K (L-N $_2$).

Temperature control is implemented through nitrogen gas from the Bruker VT interface. Heated or cooled gas can circulate in the shuttling tube during the sample transfer process. So even though the sample is being shuttled, temperature control is maintained and calibrated through the VT unit accordingly. We have performed experiments at sample temperatures between 0 and 50°C (all measurements presented here are at RT).

We designed two exchangeable magnetic field control units coupled with the pneumatic shuttling system to sweep polarization transfer fields from sub- μ T to hundreds of mT. These can be used to characterize field dependence of a vast array of SABRE target substrates and SABRE catalysts. For proton SABRE, we built a 16.5 mT/A solenoid that allows for straightforward field sweeps from -40 mT to +40 mT with a 180 W power supply (See Supporting Information S3). For heteronuclear SABRE (SABRE in SHield Enables Alignment Transfer to Heteronuclei, SABRE-SHEATH)[8,48], a single-layer solenoid around the shuttling tube to allow for tuning of microtesla/milligauss magnetic fields inside of mu-metal shielding.

A 3D-printed scaffold allows for either a mu-metal magnetic shield (Magnetic Shield Corp. ZG-206) or the 165 G/A solenoid to be easily affixed around the shuttling tube above the bore of the magnet. In **Figure 1a**, the complete experimental setup is depicted. A CAD rendering showing the individual components of the pneumatic shuttling scheme is shown in **Figure 1b**. The modular and simple design of the pneumatic shuttling allows for transfer of the shuttle to any standard NMR magnet. The magnetic fields above the magnet and possible field sweep profiles (both μ T or mT range) can be controlled with an Arduino. Using a TTL start trigger, the Arduino can be programmed and synchronized with any desired pulse sequence to run multiple series of experiments on single SABRE substrates with full automation.

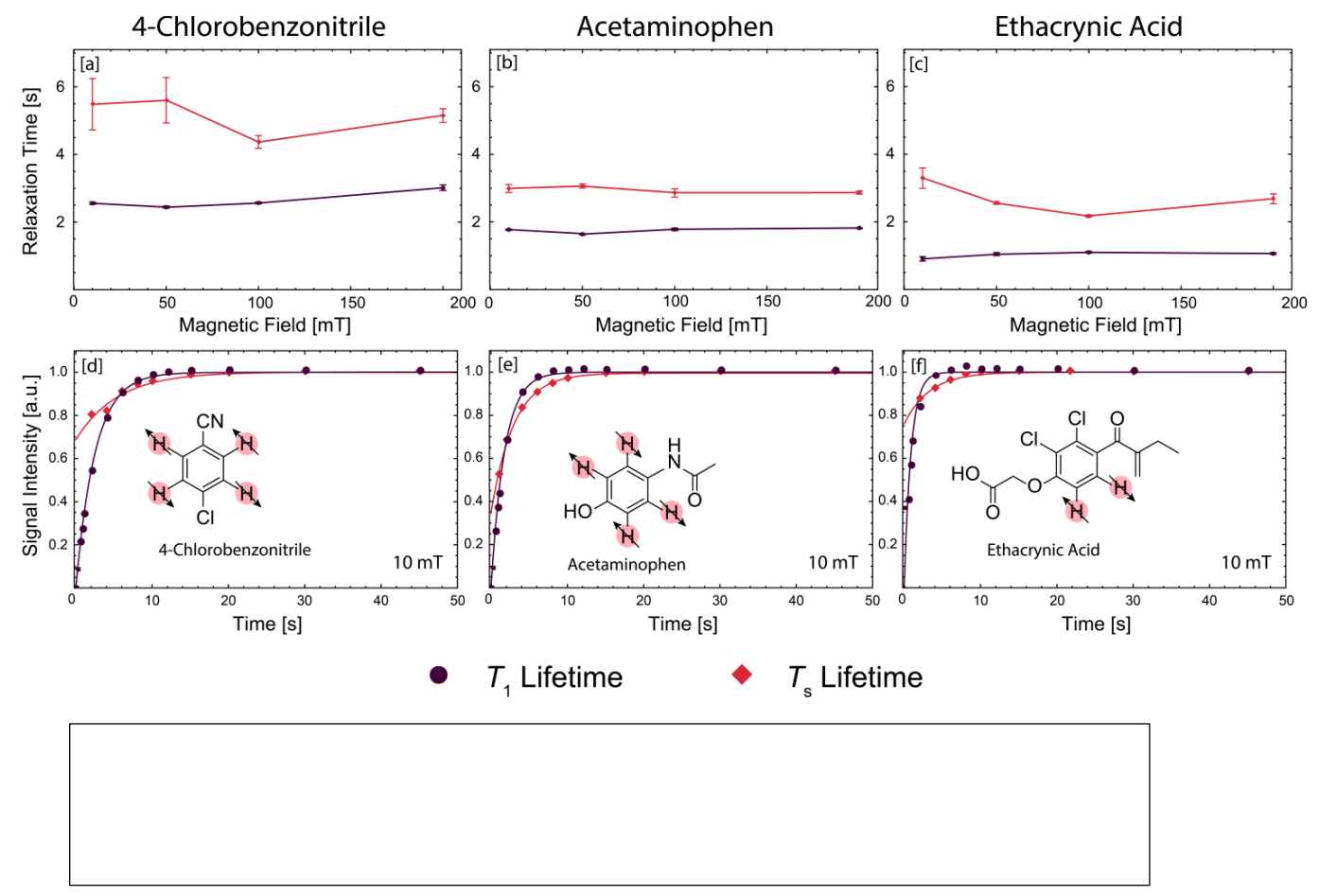
3. Results and Discussion

 We demonstrate the application of pneumatic shuttling for a variety of applications, including variable field measurements, optimization of SABRE, and hyperpolarized multidimensional experiments, elucidating new SABRE binding mechanisms.

a. Magnetization (T_1) and Singlet State Lifetime (T_S) Measurements at Variable Field

Lifetime measurements allow for substrate characterization and are important in the search for long-lived states that can be used for applications such as biomedical imaging and slow biomolecular dynamics.

Here we use field-cycling with the pneumatic shuttle to probe long-lived singlet states in 4-chlorobenzonitrile, acetaminophen, and ethacrynic acid. These molecules all contain isolated proton spin pairs on an aromatic ring, referred to as "ortho pairs" in this publication. As a simple model compound, we chose 4-chlorobenzonitrile. However "ortho pairs" also appear in common drugs such as acetaminophen, a common analgesic, and ethacrynic acid, a common diuretic. We investigate lifetimes at low magnetic fields close to standard proton SABRE hyperpolarization fields [30]. We measured T_1 relaxation rates with a standard inversion recovery experiment. A selective π -pulse is applied on the "ortho pair" and the sample subsequently shuttled to the target magnetic field for variable time intervals. Singlet lifetimes were determined by a selective π -pulse on only one of the "ortho pair" protons prior to shuttling to the target magnetic fields. In these experiments the "ortho pair" starts in the $I_{1z}+I_{2z}$ state, with selective inversion on one of the spins giving a $I_{1z}-I_{2z}$ state. The sample is then adiabatically transferred to a low magnetic field, where the "ortho pair" evolves into an $I_1\cdot I_2$ singlet state. After a variable time delay the sample subsequently undergoes adiabatic transfer to high field and the relaxation in the $I_1\cdot I_2$ is probed by a 90-degree pulse [48,49].



Both 4-chlorobenzonitrile and ethacrynic acid exhibit a strong singlet lifetime field dependence as shown in **Figure 2 a,c**. In contrast, acetaminophen (**Fig. 2 b**) exhibits much lower field dependence in both the fast and slow relaxation rates. This is most likely due to the protons on the secondary amine and the alcohol, which induce dipolar relaxation effects with weak field dependence. In contrast, there are no nearby protons on the 4-Cbn and EA.

b. Field and Polarization Buildup Optimization

SABRE hyperpolarization has a range of optimum transfer fields due to variation in scalar couplings dependent on substrate [50,51]. In the following we present field sweeps to find the optimum polarization transfer fields.

To sweep from – 40 mT to +40 mT, we use the custom built 16.5 mT/A coil. In **Figure 3b**, we present a completely automated optimization of the polarization transfer field for [14 N]-pyridine. The coil is swept in 2 mT increments from -30 mT to +30 mT, to find the optimum polarization transfer fields for the different protons. The maximum 1 H polarization observed for [14 N]-pyridine is 2.9%. We find the optimum polarization transfer field for the ortho protons at \sim ±7 mT, in agreement with literature reported values [10]. A more accurate polarization transfer field can easily be determined through a field sweep with a smaller step size.

A mu-metal shield can be used to access the μT regime for SABRE-SHEATH, but precise optimization of the level anti-crossing field requires fine tuning with an additional solenoid [8,52,53]. A single-layer solenoid inside the mu-metal

shield is swept from -7.0 to +7.0 μ T with 0.5 μ T steps. **Figure 3a** displays a field optimization for SABRE-SHEATH of [^{15}N]-pyridine. Due to residual magnetization of the shields, there is an offset of -1.5 μ T in the x-axis. The plot shows the maximum polarization for [^{15}N]-pyridine at -0.5 μ T, which corresponds to an actual field of +1.0 μ T. The maximum polarization observed for ^{15}N -pyridine is 0.5%. The data was acquired with full automation using the pneumatic shuttle and the overall experiment run time for such a field sweep is ~40 min. In previous experiments, manual field sweeps required an entire day.

The polarization buildup on different substrates and nuclei can be easily determined with shuttling. **Figure 3 c,d** show the polarization buildup curves in 1H SABRE and ^{15}N SABRE-SHEATH for $[^{15}N]$ -pyridine. The polarization buildup is measured by varying the p- H_2 bubbling time. The maximum polarization observed in the bubbling optimization is 0.1% for ^{15}N and 0.3% for 1H in $[^{15}N]$ -pyridine. The displayed standard deviations are obtained from four shuttling experiments run in sequence. These indicate the reproducibility of the automated pneumatic shuttling.

Fits are calculated with a limited exponential growth equation, with B and τ as the dead time and characteristic polarization build-up time, respectively. B is the time it takes before polarization build-up for ^{15}N is $\sim 1.5 x$ faster than ^{1}H at the respective polarization transfer fields of 6.5 mT and 1.0 μ T. Already 85% of the maximum SABRE polarization is achieved after only 23 s of p-H $_2$ bubbling for ^{15}N (**Fig. 3c**) and 38 s for ^{1}H (**Fig. 3d**).

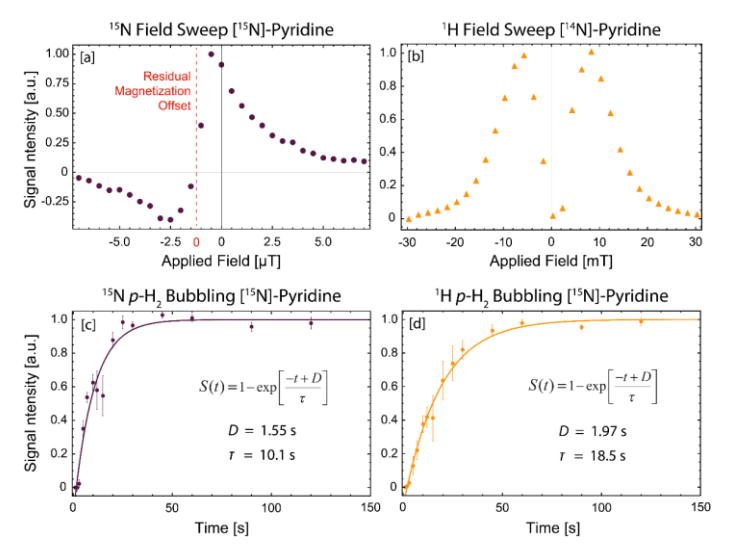


Fig. 3 Polarization transfer field optimization and polarization buildup for a [IMes+Py] sample. **(a)** Field sweep from -7.0 to +7.0 μ T (0.5 μ T steps) to optimize ¹⁵N SABRE-SHEATH; **(b)** Field sweep from -30 to +30 mT (2 mT steps) to optimize ¹H SABRE; **(c)** SABRE-SHEATH polarization buildup on (¹⁵N)-pyridine and **(d)** ¹H SABRE polarization buildup on (¹⁵N)-pyridine. Polarization buildup is characterized by a time constant, τ , and the dead time before polarization buildup, *B*.

Buildup rates depend on the *J*-coupling network, transfer field, chemical exchange, p-H₂ delivery, and T_1 relaxation [54]. As the chemical system is the same for ¹⁵N (**Fig. 3c**) and ¹H (**Fig. 3d**), the observed difference in polarization buildup rate can only be attributed to differences in *J*-coupling across the SABRE complex and relaxation rates at the respective SABRE transfer fields.

Notably, we can achieve high reproducibility of polarization buildup of pyridine with only a small deviation between experiments. Shown in **Figure 3d**, we observe a standard deviation of 2% for maximum polarization achieved at 45s of bubbling. This reproducibility between experiments is already a significant improvement over existing approaches using hand-held magnet arrays [32], with these methods observing deviations of over 5% between experiments. Additionally, the 2% observed deviation in our pneumatic system is also an improvement over other automated methods such as the 5% deviation observed in stopped flow re-polarization [55].

c. Multidimensional SABRE: Inverse 15N/1H HSQC and 1H COSY

Elucidation of binding mechanisms and kinetics of the SABRE process can be difficult due to varying exchange times, catalytic intermediate mechanisms, and binding conformations with varied SABRE substrates. It appears appealing to use hyperpolarized 2D NMR to understand the detailed mechanisms. Existing hyperpolarized multidimensional techniques include ultrafast methods using spatial encoding for analysis of substrates at low concentration [56,57]. Additionally, automated stopped flow methods have been utilized to generate SABRE-hyperpolarized high-field ¹H [41] and low-field ¹H-¹³C spectroscopy [58]. In our experiments we can use pneumatic field cycling to create reproducible hyperpolarization (as already show in **Fig. 3c,d**), notably acquiring the first inverse ¹⁵N/¹H HSQC using SABRE hyperpolarization. In a multidimensional experiment, each scan (line in the indirect dimension) can have high SNR from a full SABRE hyperpolarization cycle. Therefore, averaging can be used instead of spatial encoding and low concentration SABRE catalytic species can be observed. In general, pneumatic shuttling also enables

implementation of SABRE with other multidimensional schemes such as imaging (e.g. RARE) or diffusion experiments (e.g. DOSY).

c.1. Mixed Pyridine/Acetonitrile Systems

 Here, the implemented hyperpolarized multidimensional pulse sequences give spectra that identify bound species in the SABRE complex. In **Fig. 4**, an inverse 15 N/ 1 H HSQC is displayed using 15 N hyperpolarization at microtesla fields. Detection occurs on 15 N using a double INEPT sequence to transfer hyperpolarization from 15 N to 1 H and then back to 15 N. In these experiments we observe significant "hyperpolarization T_1 noise", derived from variability in polarization levels between each scan in the indirect dimension.

In these INEPT experiments, control of the time delay for polarization transfer, $\tau = \frac{1}{4J(\mathrm{XH})}$, shows different correlations, elucidating different molecular connectivities. In a sample of 10:3, [¹⁵N]-Pyridine (Py) : [¹⁴N]-Acetonitrile (AcN) and $J(\mathrm{XH})$ set to 1.5 Hz shows only the correlation between the weakly coupled acetonitrile ¹⁵N and methyl protons (**Fig. 4a**). In contrast, increasing the $J(\mathrm{XH})$ to 11 Hz accesses correlations across the SABRE complex (**Fig. 4b**). Notably, in this second experiment, correlation peaks are seen between the ¹⁵N signal of free acetonitrile $\delta(¹⁵N)=262$ ppm and proton peaks from both free acetonitrile $\delta(¹⁴H)=2.08$ ppm and free pyridine $\delta(¹H)=8.50$ to 7.46 ppm due to spin evolution on the complex. In addition, the bound peak of the pyridine orthoprotons $\delta(^†H)=8.23$ ppm correlates to the peak of the bound acetonitrile $\delta(^{¹⁵N})=213$ ppm. This specific correlation supports higher stability of the mixed acetonitrile-pyridine complex (shown as inset in **Fig. 4a,b**) as opposed to the potential acetonitrile only complex [59].

In **Figure 4c,d**, an analogous protocol is used to analyze hydrides from the SABRE complex, by scanning a different 1 H range in the indirect dimension. In the spectrum of **Fig. 4c**, both correlations and peak phase between acetonitrile (free & bound) and the proton hydride peaks help with hydride peak assignment observed in the single-scan spectra (**Fig. 4d**) as explained in the following. The hydride trans to the acetonitrile is expected to have a stronger correlation to the 15 N than the cis-hydride. This is due to stronger trans *J*-couplings relative to cis *J*-couplings. We observe these stronger correlations between free acetonitrile the trans hydrides at $\delta(^1\text{H})$ =-20.6 ppm and -21.1 ppm. The broad peak at $\delta(^1\text{H})$ =-20.6 ppm is due to the short lifetime of the $[^{15}\text{N}]$ -AcN/CD₃OD complex.

Furthermore, we can also use the phase of the peaks to differentiate cis and trans hydrides. Here, the observed phase difference in the correlations between the hydrides and bound acetonitrile at $\delta(^{15}N)=213$ ppm indicate the cis or trans position. Specifically, the in-phase peak at $\delta(^{1}H)=-21.1$ ppm corresponds to the cis hydride position and antiphase peak at $\delta(^{1}H)=-24.4$ ppm corresponds to the trans hydride position. Fundamentally, this is due to the greater spin evolution of the trans hydrides relative to the cis hydrides.

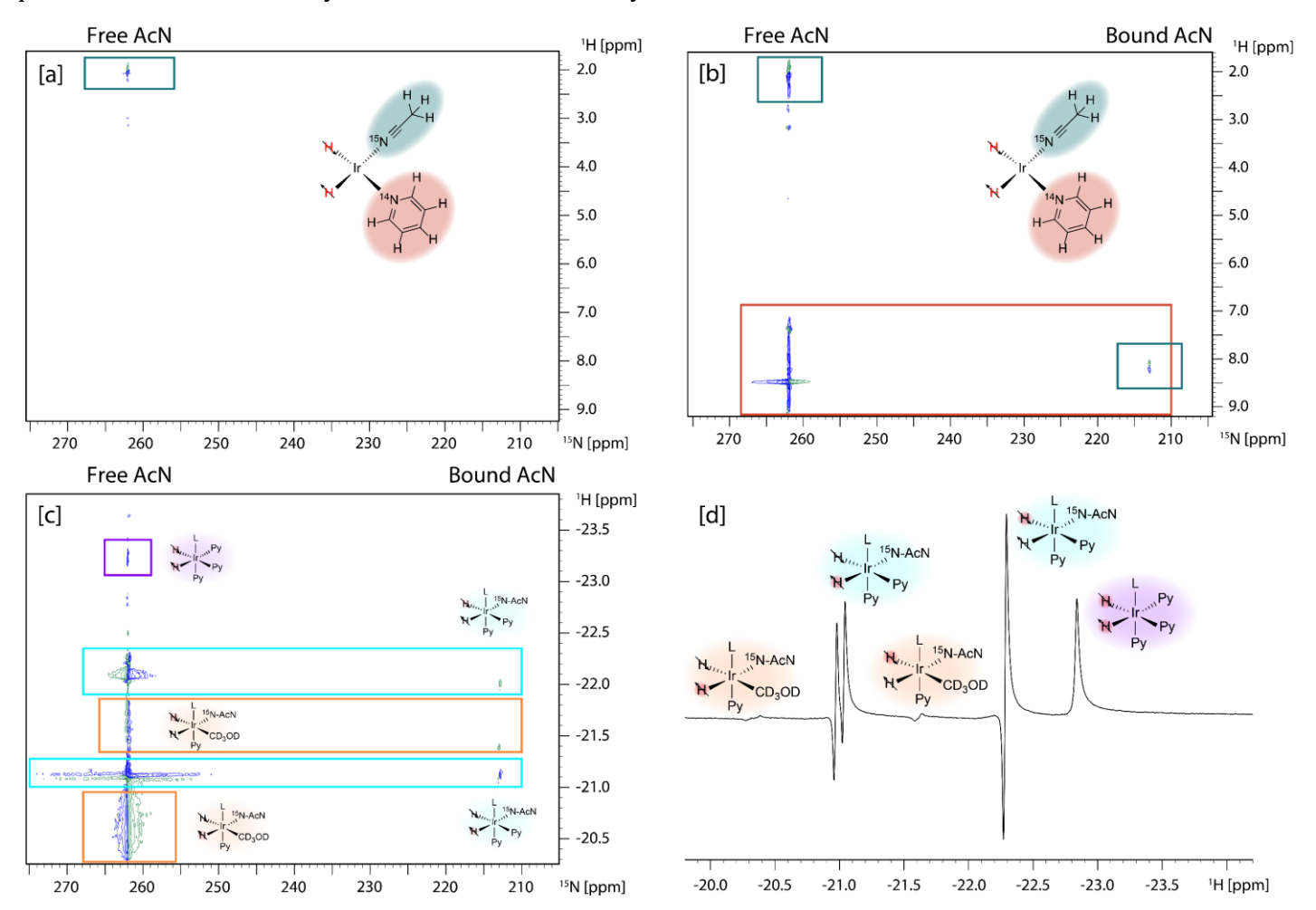


Fig. 4 Hyperpolarized spectra of IMes+ 15 N-acetonitrile (3eq)+ 14 N-pyridine (10eq) acquired with pneumatic shuttling. **(a-c)** 128 scan SABRE hyperpolarized 2D-spectra using pneumatic shuttling; **(a)** Inverse 15 N/ 1 H HSQC with J(XH)=1.5 Hz, showing only correlation with the short-range coupled AcN methyl protons; **(b)** Inverse 15 N/ 1 H HSQC with J(XH)=11 Hz, showing correlation of both the unbound (262 ppm) and bound (213 ppm) AcN 15 N to both the AcN methyl and pyridine protons; **(c)** Inverse 15 N/ 1 H of the hydride region of the proton spectra, showing correlations of the AcN/Py hydride region correlated to the bound and unbound 15 N-AcN. **(d)** One dimensional 1 H spectra of the hydride region with peaks assigned to SABRE hydrides using corresponding multidimensional spectra.

c.2. Metronidazole Systems

 Hyperpolarized multidimensional NMR can also be applied to single substrate systems to extract information about chemical exchange and spin dynamics. Here we illustrate this with the common antibiotic metronidazole (Inset, Fig. 5a), a promising SABRE substrate due to its high polarization (~20%) long relaxation times (~8 min) [60,61]. Multidimensional SABRE hyperpolarized NMR using pneumatic shuttling elucidates additional binding modes of metronidazole. In Fig. 5a, multiple bound states can be observed from 5.5 to 7.0 ppm in an inverse ¹⁵N/¹H HSOC. Specifically, these correlations are between the bound metronidazole protons and the imidazole ¹⁵N spins (labeled X and Y, inset, Fig. 5a). For example, the peak at $\delta(^{1}H)=4.2$ ppm and $\delta(^{15}N)=273$ ppm is a correlation between C2 and X (see inset), which speaks to binding of the OH to the Ir center, especially because we do not observe a correlation between C2 and Y. We conclude that this correlation is a result of additional J-couplings across the iridium due to bidentate binding of both the imidazole nitrogen and alcohol.

Finally, we also demonstrate 1H COSY of ($^{15}N_2$)-metronidazole with pre-polarization on 1H at 6.5 mT, as shown in **Fig. 5b**. Here, peaks can be observed that are difficult to resolve in a 1D SABRE experiment, due to the peak intensity and crowding with many bound species. For example, the mesitylene CH_3 peaks from IMes binding to Ir (-0.15 ppm) are easily identifiable by strong correlations to the A, B, and C1 protons of metronidazole (see inset).

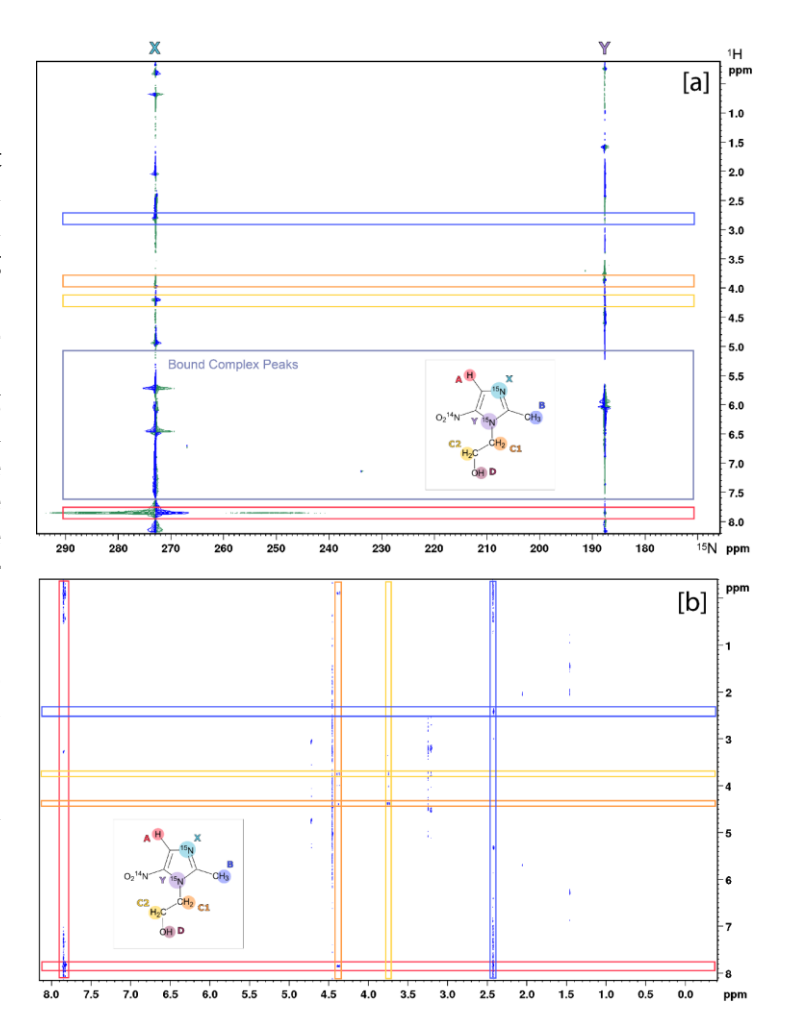


Fig. 5 IMes (3mM) + 15 N₂-Metronidazole (30mM) in CD₃OD **(a)** Inverse 15 N/ 1 H HSQC with J(XH)=1.5 Hz, showing spin correlations in metronidazole (colored and noted) as well as bound states not discernable in single-scan hyperpolarized spectra. **(b)** 1 H COSY showing correlations across the SABRE complex in both bound and free metronidazole states, as well as to other coordinating compounds (H₂O, CH₃OH).

These experiments show how the designed pneumatic shuttling-enabled multidimensional spectra can unveil new polarization transfer and chemical exchange mechanisms in the SABRE process.

4. Conclusion

The described pneumatic shuttling method provides a simple, inexpensive way to construct a field cycling apparatus. This apparatus is shown for use with non-hyperpolarized (thermally polarized) and parahydrogen hyperpolarized samples. In both cases variable field experiments were performed for studies of field-dependent singlet state lifetimes and SABRE hyperpolarization dynamics respectively. In the thermally polarized field-cycling measurements of T_1 , fitting errors are consistently below 0.1 s. With parahydrogen, we access hyperpolarized multidimensional spectroscopy and acquire hyperpolarized 15 N/ 1 H HSQC experiments to shed light onto unexplored SABRE substrate-catalyst binding interactions. While hyperpolarized ultrafast multidimensional methods allow fast acquisition and chemical characterization at low concentrations [41,56], our shuttling hyperpolarized HSQC spectra do not sacrifice signal-to-noise for spatio-spectral encoding and take advantage of the full signal-to-noise gain afforded by hyperpolarization. Here we use the signal gain to identify and assign hydride species in a mixed SABRE complex, which was enabled by 2D correlations between these hydrides and exchanging substrates. In addition, 2D correlations assist the discovery of unexpected binding modes of metronidazole to the Ir metal center through its hydroxyl group.

In summary, the pneumatic shuttle is simple to adapt and enables field-cycling of thermally polarized samples as well as hyperpolarized samples with continuously regenerated hyperpolarization. The system can access wide field ranges by operation with electromagnets, static magnet arrays, or magnetic shielding. In the 2D spectra a remaining issue is relatively strong "hyperpolarized T_1 noise" stemming from slight inconsistencies in the regenerated hyperpolarization in each indirect line. Future possibilities include, field cycling with hydrogenative PHIP, field dependent studies of CIDNP, multidimensional NMR at higher than 2 dimensions, incorporation of non-uniform sampling for significant speed-up with given hyperpolarized signals. These approaches can be expected to be of use for characterization of hyperpolarization mechanisms, and eventually hyperpolarized biomolecular structures and their dynamics.

5. Experimental Methods

Sample preparation: A solution of 4.7 mmol pre-catalyst [Ir(IMes)(COD)Cl] (IMes = 1,3-bis(2,4,6-trimethylphenyl)imidazol-2-ylidene, COD= 1,5-cyclooctadiene) in CD₃OD (Cambridge Isotope Laboratories) is combined with 12.3 M (15 N)-Pyridine or 18.7 M (15 N)-Acetonitrile to reach a final concentration of 47 mmol of substrate (10 eq) under inert gas (Ar) conditions. 750 μ L of the solution are pipetted into a 7" medium wall pressure NMR tube (Wilmad 524-PV-7). The catalyst is activated with a low flow of p-H₂ (15 min at 25°C and 100 psi) bubbled through the solution.

6. Acknowledgments

This work has been supported by funding from North Carolina State University and NIH R21-EB025313. In addition, we acknowledge funding from the North Carolina Biotechnology Center as well as the Mallinckrodt Foundation. EYC thanks NSF CHE-1904780 and NCI 1R21CA220137. The authors have no competing financial interests.

7. References

- [1] P. Nikolaou, B.M. Goodson, E.Y. Chekmenev, NMR hyperpolarization techniques for biomedicine, Chem. A Eur. J. 21 (2015) 3156–3166. https://doi.org/10.1002/chem.201405253.
- [2] J.H. Ardenkjaer-Larsen, G.S. Boebinger, A. Comment, S. Duckett, A.S. Edison, F. Engelke, C. Griesinger, R.G. Griffin, C. Hilty, H. Maeda, G. Parigi, T. Prisner, E. Ravera, J. Van Bentum, S. Vega, A. Webb, C. Luchinat, H. Schwalbe, L. Frydman, Facing and Overcoming Sensitivity Challenges in Biomolecular NMR Spectroscopy, Angew. Chemie Int. Ed. 54 (2015) 9162–9185. https://doi.org/10.1002/anie.201410653.
- [3] J. Hovener, A.N. Pravdivtsev, B. Kidd, C.R. Bowers, S. Glöggler, K. V Kovtunov, M. Plaumann, R. Katz-Brull, K. Buckenmaier, A. Jerschow, F. Reineri, T. Theis, R. V Shchepin, S. Wagner, N.M.M. Zacharias, P. Bhattacharya, E.Y. Chekmenev, Parahydrogen-based Hyperpolarization for Biomedicine, Angew. Chemie Int. Ed. (2018). https://doi.org/10.1002/anie.201711842.
- [4] S.B. Duckett, R.E. Mewis, Application of para hydrogen induced polarization techniques in NMR spectroscopy and imaging, Acc. Chem. Res. 45 (2012) 1247–1257. https://doi.org/10.1021/ar2003094.
- [5] C.R. Bowers, D.P. Weitekamp, Transformation of symmetrization order to nuclear-spin magnetization by chemical reaction and nuclear magnetic resonance, Phys. Rev. Lett. 57 (1986) 2645–2648. https://doi.org/10.1103/PhysRevLett.57.2645.
- [6] R.W. Adams, J.A. Aguilar, K.D. Atkinson, M.J. Cowley, P.I.P. Elliott, S.B. Duckett, G.G.R. Green, I.G. Khazal, J. Lopez-Serrano, D.C. Williamson, Reversible Interactions with para-Hydrogen Enhance NMR Sensitivity by Polarization Transfer, Science (80-.). 323 (2009) 1708–1711. https://doi.org/10.1126/science.1168877.
- [7] P.J. Rayner, S.B. Duckett, Signal Amplification by Reversible Exchange (SABRE): From Discovery to Diagnosis, Angew. Chemie Int. Ed. 57 (2018) 6742–6753. https://doi.org/10.1002/anie.201710406.
- [8] T. Theis, M.L. Truong, A.M. Coffey, R. V. Shchepin, K.W. Waddell, F. Shi, B.M. Goodson, W.S. Warren, E.Y. Chekmenev, Microtesla SABRE enables 10% nitrogen-15 nuclear Spin polarization, J. Am. Chem. Soc. 137 (2015) 1404–1407. https://doi.org/10.1021/ja512242d.
- [9] P.J. Rayner, M.J. Burns, A.M. Olaru, P. Norcott, M. Fekete, G.G.R. Green, L.A.R. Highton, R.E. Mewis, S.B. Duckett, Delivering strong 1 H nuclear hyperpolarization levels and long magnetic lifetimes through signal amplification by reversible exchange, Proc. Natl. Acad. Sci. 114 (2017) E3188–E3194. https://doi.org/10.1073/pnas.1620457114.
- [10] M.J. Cowley, R.W. Adams, K.D. Atkinson, M.C.R. Cockett, S.B. Duckett, G.G.R. Green, J.A.B. Lohman, R. Kerssebaum, D. Kilgour, R.E. Mewis, Iridium N-heterocyclic carbene complexes as efficient catalysts for magnetization transfer from para -hydrogen, J. Am. Chem. Soc. 133 (2011) 6134–6137. https://doi.org/10.1021/ja200299u.
- [11] B.E. Kidd, J.L. Gesiorski, M.E. Gemeinhardt, R. V. Shchepin, K. V. Kovtunov, I. V. Koptyug, E.Y. Chekmenev, B.M. Goodson, Facile Removal of Homogeneous SABRE Catalysts for Purifying Hyperpolarized Metronidazole, a Potential Hypoxia Sensor, J. Phys. Chem. C. 122 (2018) 16848–16852. https://doi.org/10.1021/acs.jpcc.8b05758.
- [12] S.S. Roy, K.M. Appleby, E.J. Fear, S.B. Duckett, SABRE-Relay: A Versatile Route to Hyperpolarization, J. Phys. Chem. Lett. 9 (2018) 1112–1117. https://doi.org/10.1021/acs.jpclett.7b03026.
- [13] R. V. Shchepin, M.L. Truong, T. Theis, A.M. Coffey, F. Shi, K.W. Waddell, W.S. Warren, B.M. Goodson, E.Y. Chekmenev, Hyperpolarization of "Neat" Liquids by NMR Signal Amplification by Reversible Exchange, J. Phys. Chem. Lett. 6 (2015) 1961–1967. https://doi.org/10.1021/acs.jpclett.5b00782.
- [14] J.F.P. Colell, M. Emondts, A.W.J. Logan, K. Shen, J. Bae, R. V. Shchepin, G.X. Ortiz, P. Spannring, Q. Wang, S.J. Malcolmson, E.Y. Chekmenev, M.C. Feiters, F.P.J.T. Rutjes, B. Blümich, T. Theis, W.S. Warren, Direct Hyperpolarization of Nitrogen-15 in Aqueous Media with Parahydrogen in Reversible Exchange, J. Am. Chem. Soc. 139 (2017) 7761–7767. https://doi.org/10.1021/jacs.7b00569.

- [15] W. Iali, P.J. Rayner, S.B. Duckett, Using parahydrogen to hyperpolarize amines, amides, carboxylic acids, alcohols, phosphates, and carbonates, Sci. Adv. 4 (2018) 1–7. https://doi.org/10.1126/sciadv.aao6250.
- [16] T. Theis, M. Truong, A.M. Coffey, E.Y. Chekmenev, W.S. Warren, LIGHT-SABRE enables efficient in-magnet catalytic hyperpolarization, J. Magn. Reson. 248 (2014) 23–26. https://doi.org/10.1016/j.jmr.2014.09.005.
- [17] K.L. Ivanov, A.N. Pravdivtsev, A. V. Yurkovskaya, H.M. Vieth, R. Kaptein, The role of level anti-crossings in nuclear spin hyperpolarization, Prog. Nucl. Magn. Reson. Spectrosc. 81 (2014) 1–36. https://doi.org/10.1016/j.pnmrs.2014.06.001.

- [18] A.N. Pravdivtsev, A. V. Yurkovskaya, H.M. Vieth, K.L. Ivanov, R. Kaptein, Level anti-crossings are a key factor for understanding para-hydrogen-induced hyperpolarization in SABRE experiments, ChemPhysChem. 14 (2013) 3327–3331. https://doi.org/10.1002/cphc.201300595.
- [19] K.L. Ivanov, A. V. Yurkovskaya, H.M. Vieth, Coherent transfer of hyperpolarization in coupled spin systems at variable magnetic field, J. Chem. Phys. 128 (2008). https://doi.org/10.1063/1.2901019.
- [20] L. Buljubasich, M.B. Franzoni, H.W. Spiess, K. Münnemann, Level anti-crossings in ParaHydrogen Induced Polarization experiments with Cs-symmetric molecules, J. Magn. Reson. 219 (2012) 33–40. https://doi.org/10.1016/j.jmr.2012.03.020.
- [21] J.B. Hövener, N. Schwaderlapp, T. Lickert, S.B. Duckett, R.E. Mewis, L.A.R. Highton, S.M. Kenny, G.G.R. Green, D. Leibfritz, J.G. Korvink, J. Hennig, D. Von Elverfeldt, A hyperpolarized equilibrium for magnetic resonance, Nat. Commun. 4 (2013) 1–5. https://doi.org/10.1038/ncomms3946.
- [22] J.B. Hövener, N. Schwaderlapp, R. Borowiak, T. Lickert, S.B. Duckett, R.E. Mewis, R.W. Adams, M.J. Burns, L.A.R. Highton, G.G.R. Green, A. Olaru, J. Hennig, D. Von Elverfeldt, Toward biocompatible nuclear hyperpolarization using signal amplification by reversible exchange: Quantitative in situ spectroscopy and high-field imaging, Anal. Chem. 86 (2014) 1767–1774. https://doi.org/10.1021/ac403653q.
- [23] J.B. Hövener, S. Knecht, N. Schwaderlapp, J. Hennig, D. Von Elverfeldt, Continuous re-hyperpolarization of nuclear spins using parahydrogen: Theory and experiment, ChemPhysChem. 15 (2014) 2451–2457. https://doi.org/10.1002/cphc.201402177.
- [24] N. Eshuis, R.L.E.G. Aspers, B.J.A. Van Weerdenburg, M.C. Feiters, F.P.J.T. Rutjes, S.S. Wijmenga, M. Tessari, 2D NMR Trace Analysis by Continuous Hyperpolarization at High Magnetic Field, Angew. Chemie - Int. Ed. 54 (2015) 14527–14530. https://doi.org/10.1002/anie.201507831.
- [25] S. Knecht, A.S. Kiryutin, A. V. Yurkovskaya, K.L. Ivanov, Re-polarization of nuclear spins using selective SABRE-INEPT, J. Magn. Reson. 287 (2018) 10–14. https://doi.org/10.1016/j.jmr.2017.12.010.
- [26] A.N. Pravdivtsev, A. V. Yurkovskaya, H.M. Vieth, K.L. Ivanov, RF-SABRE: A Way to Continuous Spin Hyperpolarization at High Magnetic Fields, J. Phys. Chem. B. 119 (2015) 13619–13629. https://doi.org/10.1021/acs.jpcb.5b03032.
- [27] P. Rovedo, S. Knecht, T. Bäumlisberger, A.L. Cremer, S.B. Duckett, R.E. Mewis, G.G.R. Green, M. Burns, P.J. Rayner, D. Leibfritz, J.G. Korvink, J. Hennig, G. Pütz, D. Von Elverfeldt, J.B. Hövener, Molecular MRI in the Earth's Magnetic Field Using Continuous Hyperpolarization of a Biomolecule in Water, J. Phys. Chem. B. 120 (2016) 5670–5677. https://doi.org/10.1021/acs.jpcb.6b02830.
- [28] N.K.J. Hermkens, R.L.E.G. Aspers, M.C. Feiters, F.P.J.T. Rutjes, M. Tessari, Trace analysis in water-alcohol mixtures by continuous p-H2 hyperpolarization at high magnetic field, Magn. Reson. Chem. 56 (2018) 633–640. https://doi.org/10.1002/mrc.4692.
- [29] S. Lehmkuhl, M. Wiese, L. Schubert, M. Held, M. Küppers, M. Wessling, B. Blümich, Continuous hyperpolarization with parahydrogen in a membrane reactor, J. Magn. Reson. 291 (2018) 8–13. https://doi.org/10.1016/j.jmr.2018.03.012.
- [30] A.S. Kiryutin, A. V. Yurkovskaya, H. Zimmermann, H.M. Vieth, K.L. Ivanov, Complete magnetic field dependence of SABRE-derived polarization, Magn. Reson. Chem. 56 (2018) 651–662. https://doi.org/10.1002/mrc.4694.
- [31] S.B. Duckett, R.E. Mewis, Application of para hydrogen induced polarization techniques in NMR spectroscopy and imaging, Acc. Chem. Res. 45 (2012) 1247–1257. https://doi.org/10.1021/ar2003094.
- [32] P.M. Richardson, S. Jackson, A.J. Parrott, A. Nordon, S.B. Duckett, M.E. Halse, A simple hand-held magnet array for efficient and reproducible SABRE hyperpolarisation using manual sample shaking, Magn. Reson. Chem. 56 (2018) 641–650. https://doi.org/10.1002/mrc.4687.
- [33] R.E. Mewis, K.D. Atkinson, M.J. Cowley, S.B. Duckett, G.G.R. Green, R.A. Green, L.A.R. Highton, D. Kilgour, L.S. Lloyd, J.A.B. Lohman, D.C. Williamson, Probing signal amplification by reversible exchange using an NMR flow system, Magn. Reson. Chem. 52 (2014) 358–369. https://doi.org/10.1002/mrc.4073.
- [34] P. Štěpánek, C. Sanchez-Perez, V.V. Telkki, V. V. Zhivonitko, A.M. Kantola, High-throughput continuous-flow system for SABRE hyperpolarization, J. Magn. Reson. 300 (2019) 8–17. https://doi.org/10.1016/j.jmr.2019.01.003.
- [35] L. Bordonali, N. Nordin, E. Fuhrer, N. Mackinnon, J.G. Korvink, Parahydrogen based NMR hyperpolarisation goes micro: An alveolus for small molecule chemosensing, Lab Chip. 19 (2019) 503–512. https://doi.org/10.1039/c8lc01259h.
- [36] J. Eills, W. Hale, M. Sharma, M. Rossetto, M.H. Levitt, M. Utz, High-Resolution Nuclear Magnetic Resonance Spectroscopy with Picomole Sensitivity by Hyperpolarization on a Chip, J. Am. Chem. Soc. 141 (2019) 9955–9963. https://doi.org/10.1021/jacs.9b03507.
- [37] C.Y. Chou, M. Chu, C.F. Chang, T.H. Huang, A compact high-speed mechanical sample shuttle for field-dependent high-resolution solution NMR, J. Magn. Reson. 214 (2012) 302–308. https://doi.org/10.1016/j.jmr.2011.12.001.
- [38] D.A. Barskiy, K. V. Kovtunov, I. V. Koptyug, P. He, K.A. Groome, Q.A. Best, F. Shi, B.M. Goodson, R. V. Shchepin, M.L. Truong, A.M. Coffey, K.W. Waddell, E.Y. Chekmenev, In situ and ex situ low-field NMR spectroscopy and MRI endowed by SABRE hyperpolarization, ChemPhysChem. 15 (2014) 4100–4107. https://doi.org/10.1002/cphc.201402607.
- [39] V. Daniele, F.X. Legrand, P. Berthault, J.N. Dumez, G. Huber, Single-Scan Multidimensional NMR Analysis of Mixtures at Sub-Millimolar Concentrations by using SABRE Hyperpolarization, ChemPhysChem. 16 (2015) 3413–3417. https://doi.org/10.1002/cphc.201500535.
- [40] A.S. Kiryutin, G. Sauer, D. Tietze, M. Brodrecht, S. Knecht, A. V. Yurkovskaya, K.L. Ivanov, O. Avrutina, H. Kolmar, G. Buntkowsky, Ultrafast Single-Scan 2D NMR Spectroscopic Detection of a PHIP-Hyperpolarized Protease Inhibitor, Chem. A Eur. J. 25 (2019) 4025–4030. https://doi.org/10.1002/chem.201900079.
- [41] L.S. Lloyd, R.W. Adams, M. Bernstein, S. Coombes, S.B. Duckett, G.G.R. Green, R.J. Lewis, R.E. Mewis, C.J. Sleigh, Utilization of SABRE-derived hyperpolarization to detect low-concentration analytes via 1D and 2D NMR methods, J. Am. Chem. Soc. 134 (2012) 12904–12907. https://doi.org/10.1021/ja3051052.
- [42] I. V. Zhukov, A.S. Kiryutin, A. V. Yurkovskaya, Y.A. Grishin, H.M. Vieth, K.L. Ivanov, Field-cycling NMR experiments in an ultra-wide

magnetic field range: Relaxation and coherent polarization transfer, Phys. Chem. Chem. Phys. 20 (2018) 12396–12405. https://doi.org/10.1039/c7cp08529j.

- [43] M.G. Pravica, D.P. Weitekamp, Net NMR alignment by adiabatic transport of parahydrogen addition products to high magnetic field, Chem. Phys. Lett. 145 (1988) 255–258. https://doi.org/10.1016/0009-2614(88)80002-2.
- [44] A. Bielecki, D.B. Zax, K.W. Zilm, A. Pines, Zero-field NMR and NQR spectrometer, Rev. Sci. Instrum. 57 (1986) 393–403. https://doi.org/10.1063/1.1138898.
- [45] M.C.D. Tayler, T. Theis, T.F. Sjolander, J.W. Blanchard, A. Kentner, S. Pustelny, A. Pines, D. Budker, Invited Review Article: Instrumentation for nuclear magnetic resonance in zero and ultralow magnetic field, Rev. Sci. Instrum. 88 (2017) 091101. https://doi.org/10.1063/1.5003347.
- [46] A. Bornet, S. Jannin, G. Bodenhausen, Three-field NMR to preserve hyperpolarized proton magnetization as long-lived states in moderate magnetic fields, Chem. Phys. Lett. 512 (2011) 151–154. https://doi.org/10.1016/j.cplett.2011.07.015.
- [47] A. Krahn, P. Lottmann, T. Marquardsen, A. Tavernier, M.-T. Türke, M. Reese, A. Leonov, M. Bennati, P. Hoefer, F. Engelke, C. Griesinger, Shuttle DNP spectrometer with a two-center magnet, Phys. Chem. Chem. Phys. 12 (2010) 5830. https://doi.org/10.1039/c003381b.
- [48] T. Theis, G.X. Ortiz, A.W.J. Logan, K.E. Claytor, Y. Feng, W.P. Huhn, V. Blum, S.J. Malcolmson, E.Y. Chekmenev, Q. Wang, W.S. Warren, Direct and cost-efficient hyperpolarization of long-lived nuclear spin states on universal 15N2-diazirine molecular tags, Sci. Adv. 2 (2016) 1–8. https://doi.org/10.1126/sciadv.1501438.
- [49] M. Carravetta, M.H. Levitt, Long-lived nuclear spin states in high-field solution NMR, J. Am. Chem. Soc. 126 (2004) 6228–6229. https://doi.org/10.1021/ja0490931.
- [50] E.B. Dücker, L.T. Kuhn, K. Münnemann, C. Griesinger, Similarity of SABRE field dependence in chemically different substrates, J. Magn. Reson. 214 (2012) 159–165. https://doi.org/10.1016/j.jmr.2011.11.001.
- [51] H. Zeng, J. Xu, J. Gillen, M.T. McMahon, D. Artemov, J.M. Tyburn, J.A.B. Lohman, R.E. Mewis, K.D. Atkinson, G.G.R. Green, S.B. Duckett, P.C.M. Van Zijl, Optimization of SABRE for polarization of the tuberculosis drugs pyrazinamide and isoniazid, J. Magn. Reson. 237 (2013) 73–78. https://doi.org/10.1016/j.jmr.2013.09.012.
- [52] M.L. Truong, T. Theis, A.M. Coffey, R. V. Shchepin, K.W. Waddell, F. Shi, B.M. Goodson, W.S. Warren, E.Y. Chekmenev, ¹⁵N Hyperpolarization by Reversible Exchange Using SABRE-SHEATH, J. Phys. Chem. C. 119 (2015) 8786–8797. https://doi.org/10.1021/acs.jpcc.5b01799.
- [53] J.F.P. Colell, A.W.J. Logan, Z. Zhou, R. V Shchepin, D.A. Barskiy, G.X. Ortiz, Q. Wang, S.J. Malcolmson, E.Y. Chekmenev, W.S. Warren, T. Theis, Generalizing, Extending, and Maximizing Nitrogen-15 Hyperpolarization Induced by Parahydrogen in Reversible Exchange, J. Phys. Chem. C. 121 (2017) 6626–6634. https://doi.org/10.1021/acs.jpcc.6b12097.
- [54] D.A. Barskiy, S. Knecht, A. V. Yurkovskaya, K.L. Ivanov, SABRE: Chemical kinetics and spin dynamics of the formation of hyperpolarization, Prog. Nucl. Magn. Reson. Spectrosc. 114–115 (2019) 33–70. https://doi.org/10.1016/j.pnmrs.2019.05.005.
- [55] P.M. Richardson, A.J. Parrott, O. Semenova, A. Nordon, S.B. Duckett, M.E. Halse, SABRE hyperpolarization enables high-sensitivity 1 H and 13 C benchtop NMR spectroscopy, Analyst. 143 (2018) 3442–3450. https://doi.org/10.1039/C8AN00596F.
- [56] L. Frydman, D. Blazina, Ultrafast two-dimensional nuclear magnetic resonance spectroscopy of hyperpolarized solutions, Nat. Phys. 3 (2007) 415–419. https://doi.org/10.1038/nphys597.
- [57] B. Plainchont, P. Giraudeau, J.-N. Dumez, Interleaved spatial/spectral encoding in ultrafast 2D NMR spectroscopy, J. Magn. Reson. 305 (2019) 112–121. https://doi.org/10.1016/j.jmr.2019.06.010.
- [58] A.D. Robinson, P.M. Richardson, M.E. Halse, Hyperpolarised 1 H- 13 C benchtop NMR spectroscopy, Appl. Sci. 9 (2019) 1–14. https://doi.org/10.3390/app9061173.
- [59] R.E. Mewis, R.A. Green, M.C.R. Cockett, M.J. Cowley, S.B. Duckett, G.G.R. Green, R.O. John, P.J. Rayner, D.C. Williamson, Strategies for the hyperpolarization of acetonitrile and related Ligands by SABRE, J. Phys. Chem. B. 119 (2015) 1416–1424. https://doi.org/10.1021/jp511492q.
- [60] D.A. Barskiy, R. V. Shchepin, A.M. Coffey, T. Theis, W.S. Warren, B.M. Goodson, E.Y. Chekmenev, Over 20%15N Hyperpolarization in under One Minute for Metronidazole, an Antibiotic and Hypoxia Probe, J. Am. Chem. Soc. 138 (2016) 8080–8083. https://doi.org/10.1021/jacs.6b04784.
- [61] R. V. Shchepin, L. Jaigirdar, E.Y. Chekmenev, Spin-Lattice Relaxation of Hyperpolarized Metronidazole in Signal Amplification by Reversible Exchange in Micro-Tesla Fields, J. Phys. Chem. C. 122 (2018) 4984–4996. https://doi.org/10.1021/acs.jpcc.8b00283.